Nuclear Instruments and Methods in Physics Research B 412 (2017) 58–65

Contents lists available at ScienceDirect

Nuclear Instruments and Methods in Physics Research B

journal homepage: www.elsevier.com/locate/nimb

Resolution of the carbon contamination problem in ion irradiation experiments

G.S. Was [a,*], S. Taller [a], Z. Jiao [a], A.M. Monterrosa [a], D. Woodley [a], D. Jennings [b], T. Kubley [a], F. Naab [a], O. Toader [a], E. Uberseder [a]

[a] University of Michigan, Ann Arbor, MI 48109, USA
[b] Colorado School of Mines, Golden, CO 80401, USA

ARTICLE INFO

Article history:
Received 26 July 2017
Received in revised form 28 August 2017
Accepted 29 August 2017

Keywords:
Carbon contamination
Ion irradiation
Nuclear reaction analysis
Cold trap
Plasma cleaning

ABSTRACT

The widely experienced problem of carbon uptake in samples during ion irradiation was systematically investigated to identify the source of carbon and to develop mitigation techniques. Possible sources of carbon included carbon ions or neutrals incorporated into the ion beam, hydrocarbons in the vacuum system, and carbon species on the sample and fixture surfaces. Secondary ion mass spectrometry, atom probe tomography, elastic backscattering spectrometry, and principally, nuclear reaction analysis, were used to profile carbon in a variety of substrates prior to and following irradiation with Fe^{2+} ions at high temperature. Ion irradiation of high purity Si and Ni, and also of alloy 800H coated with a thin film of alumina eliminated the ion beam as the source of carbon. Hydrocarbons in the vacuum and/or on the sample and fixtures was the source of the carbon that became incorporated into the samples during irradiation. Plasma cleaning of the sample and sample stage, and incorporation of a liquid nitrogen cold trap both individually and especially in combination, completely eliminated the uptake of carbon during heavy ion irradiation. While less convenient, coating the sample with a thin film of alumina was also effective in eliminating carbon incorporation.

1. Introduction

The application of ion irradiation to understand radiation effects in materials has been an active field of study since the 1950s. Numerous advances in our understanding of materials behavior have been made with ion irradiation including the discovery [1] and development [2] of radiation induced segregation, radiation-induced precipitation [3], void swelling [4], and radiation enhanced diffusion [5] among others. Recently, ion irradiation has gained increased attention in an effort to simulate the effects of radiation in a reactor environment. Various studies [6–8] have been conducted that show the capability of ion irradiation to qualitatively and quantitatively capture many, if not all, of the microstructure features created in reactor. The advantages of ion irradiation are many. Dose rates (typically 10^{-3} to 10^{-4} dpa/s) are much higher than under neutron irradiation (10^{-7} to 10^{-8} dpa/s) which means that 200 dpa[1] can be reached in days or weeks instead of decades. Because there is little activation, samples can be handled as if they were unirradiated, eliminating the need for the extremely high investment in time and cost connected with the use of hot cells and dedicated characterization instrumentation. Control of ion irradiation experiments is much better than experiments in reactor, and the result is that ion irradiation is 10–1000× less costly and 10–100x quicker than test reactor irradiation. Critical to the success of ion irradiation as a radiation damage simulation tool is that the ion irradiated microstructure reflects the damage created by the ions and is not influenced by external factors such as incorporation of impurities into the sample during irradiation.

Such is the case today in the radiation damage community that many laboratories are experiencing the pickup of carbon in their samples during ion irradiation. Carbon is incorporated into the irradiated microstructure, not just as a surface contaminant. The result is an alteration of the microstructure, most notably the formation of carbides, and modification of processes such as cavity evolution. Thus it is carbon incorporation into the sample over the depth of penetration of the ion beam (0.1 to several μm) that is important. Most reports come from self-ion irradiation of iron- and nickel-base alloys irradiated at high temperature. As this observation is clearly an unintended and unwanted effect, these

* Corresponding author.
E-mail addresses: jnmeditorgs@gmail.com, gsw@umich.edu (G.S. Was).

[1] dpa is displacement per atom. For a value of one dpa, every atom will, on average, be displaced once.

http://dx.doi.org/10.1016/j.nimb.2017.08.039
0168-583X/

observations are seldom published in the open literature. However, there exists substantial earlier literature documenting this occurrence. Singer et al. [9,10] addressed observations of carbon uptake in Ti implanted steel and Ni-plated substrates. They found that irradiation with Ti resulted in incorporation of C into the solid surfaces. Carbon was distributed in a diffusion-like profile from the surface inwards. Similar observations were made for Cr and Ta-implanted steels. The authors speculated [9] and later provided evidence [10] that the uptake of carbon is due to vacuum carburization in which beam-enhanced or beam-induced adsorption and dissociation of residual CO and CO_2 molecules was responsible for the incorporation of carbon and the subsequent formation of carbides. Thomas and Bauer [11] observed carbide formation on Nb surfaces during proton irradiation at 1000 K. In fact, this process has been observed in many carbide-forming metals or alloys [12–17].

The problem has also been noted by the ion beam analysis community [18]. Healy [19] reported an extensive analysis of the factors causing the buildup of carbon on samples during ion beam analysis using a deuteron beam. They collected data on carbon contamination due to various factors, including vacuum pressure, beam area, beam contamination, beam current, temperature, and residual gas in the vacuum chamber. They concluded that the hydrocarbon component of the residual gas within the analysis chamber is the source of contamination, and that the hydrocarbons are cracked by the beam and attracted to the sample. They also noted that a cold trap near the sample minimizes contamination.

The transmission electron microscopy community has also observed the contamination of samples under the electron beam. In fact, it has been a common practice to use the buildup of carbon on the front and back surfaces of a sample to estimate sample thickness. Carbon on TEM and SEM samples was observed to occur only in the area under the beam. The TEM community has mitigated the buildup of carbon through the use of plasma cleaning of the sample prior to loading into the column, and by the use of a cold-finger near the sample during observation. Thus, the contamination of carbon can occur during heavy ion irradiation, ion beam analysis with light ions or under electron irradiation in the TEM or SEM. The common theme in all of these observations is that the contamination occurs only under the beam.

An example of carbon incorporation during ion irradiation include alloy 800H irradiated with 5 MeV Fe^{2+} at a temperature of 440 °C to a damage level of 20 dpa. Fig. 1 shows composition vs. depth profiles using three different techniques. Fig. 1a shows the carbon profile from nuclear reaction analysis utilizing the $^{12}C(d,p_0)^{13}C$ reaction with a deuteron energy of 1.5 MeV. The composition profile is characterized by a 1.7 nm thick surface layer of carbon, and enrichment below the surface, a sub-surface peak at about 1000 nm, and a depression below the bulk level starting at about 1300 nm and extending deeper into the sample. A SIMS

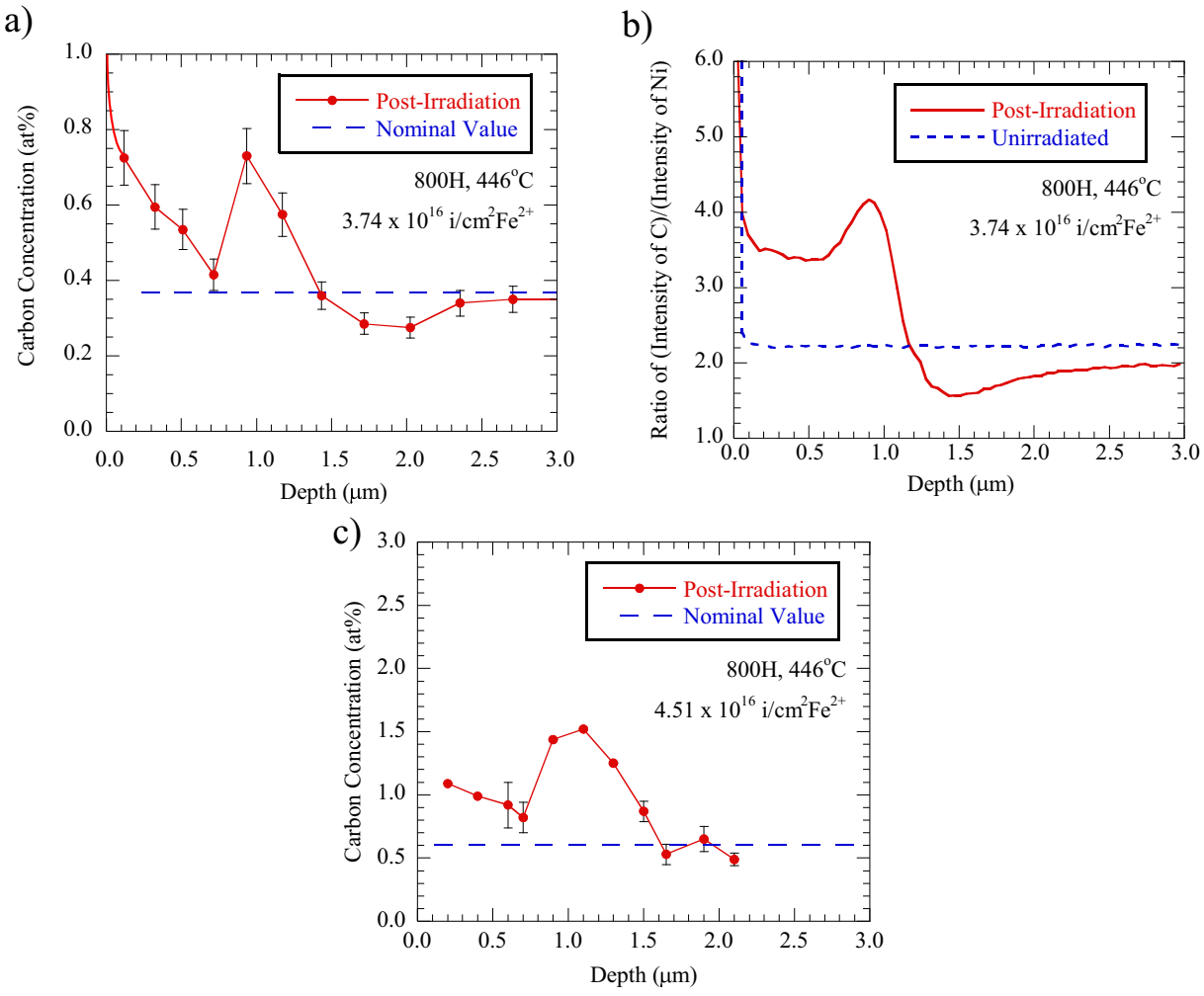

Fig. 1. Carbon concentration vs. depth profiles in alloy 800H following irradiation with 5 MeV Fe^{2+} at 446 °C to similar fluences by a) nuclear reaction analysis (4.51×10^{16} i/cm^2/17 dpa), b) secondary ion mass spectrometry (3.74×10^{16} i/cm^2/17 dpa plus He), and c) atom probe tomography (4.51×10^{16} i/cm^2/20 dpa).

profile collected on a companion sample is shown in Fig. 1b. This profile shows a very similar behavior with a surface enrichment, followed by a peak at 1000 nm and then a depression in the carbon content below the bulk level beyond about 1200 nm. Fig. 1c shows a third analysis of this irradiation condition using atom probe tomography (APT) in which tips were extracted at various depths below the surface down to 2000 nm. Here again, there is an enrichment near the surface, followed by a peak at about 800 nm and then a drop starting at about 1300 nm though in this case, it does not appear to extend below the bulk level. These data, taken using completely different techniques, are consistent in the features of the carbon profile in the subsurface following irradiation. However, they are more complicated than expected in that they show both an enrichment of carbon near the surface and what appears to be a redistribution of carbon below the surface. Carbon redistribution will be important in understanding the effects of radiation damage on the microstructure, but before this can be studied further, it must be verified by assuring that carbon uptake during irradiation is eliminated.

The following sections describe the experiments conducted to verify that carbon indeed is being incorporated during irradiation, to identify the source of the carbon, and to develop methods to eliminate its uptake. The possible sources are three: carbon in the ion beam, carbon or hydrocarbons residing on the sample surface, and carbon-containing molecules in the vacuum system. The following describes the systematic analysis of these potential sources and the development of techniques to mitigate the problem completely.

2. Experiment

Experiments were conducted on two alloys: 800H and HT9, the compositions of which are given in Table 1. HT9 is a candidate alloy for fast reactor cladding and duct components and 800H is under consideration as a potential replacement alloy for stainless steel in light water reactor core components. The nominal carbon content in alloy 800H is 0.34 ± 0.07 at.%, and for alloy HT9 it is 0.99 ± 0.20 at.%. Nuclear reaction analysis (NRA) of the as-received alloys yielded values of 0.37 ± 0.03 at.% for 800H, and 0.95 ± 0.09 at.% for HT9, where the error is a combination of uncertainties in cross section and spectrum fit, and the standard deviation of the mean of multiple measurements. Both NRA measurements are within the measurement error by chemical analysis of the alloys, thus the NRA values were used in this study. Select experiments were also conducted on single crystal silicon containing <0.06 appm C from Virginia Semiconductor, and very high purity (Falconbridge Superelectro) Ni containing 20 appm carbon.

Heavy ion irradiations were conducted using 4.4 or 5 MeV Fe^{2+} at a current density of roughly 0.5 μA/cm^2 on samples held at either 440 °C or 460 °C for alloys 800H and HT9. Irradiations were conducted with the 3.0 MV Pelletron accelerator or 1.7 MV Tandem accelerator in the Michigan Ion Beam Laboratory at the University of Michigan. The beam mode was defocused for all irradiations of HT9 with a maximum variation of 10% of the average beam current across the beam spot. The 800H was irradiated using a raster-scanned focused beam of Fe^{2+} ions at a scanning frequency of 255 Hz × 2061 Hz across the sample surface. Current was continuously monitored on the slit system that defined the irradiated region on the sample, and periodically measured by Faraday cup insertion. Samples were mounted on a copper block with a soft, thin copper foil between the sample and the block. To achieve maximum temperature control, the block was heated with a cartridge heater and also cooled by air flow through cooling tubes in the block. Sample temperature was monitored continuously using a 2-D thermal imager following calibration using type-J thermocouples at the irradiation temperature. Alloy 800H was irradiated to a fluence of either 3.95×10^{16} i/cm^2 (20 dpa) for 4.4 MeV Fe^{2+} or 4.51×10^{16} i/cm^2 for 5 MeV Fe^{2+} (20 dpa), and alloy HT9 was irradiated to a fluence of 4.47×10^{17} i/cm^2 (188 dpa), with the dpa at a depth of 600 nm from the irradiated surface, calculated using SRIM [20] in quick Kinchin-Pease mode with a displacement energy of 40 eV. The doses and temperatures were selected to produce microstructures that match those created on the same heats of the alloys irradiated in reactor. Vacuum pressure was below 1×10^{-7} torr prior to heat up. Sample heating caused the pressure to rise initially, and then decrease into the 10^{-8} torr range during irradiation.

The data in Fig. 1 refer to alloy 800H irradiated with a defocused beam consisting of 5 MeV Fe^{2+}. The sample in Fig. 1b was simultaneously irradiated with an energy degraded and raster scanned beam of He^{2+} of energy 2.15 MeV. An aluminum degrader foil of thickness 3.3 μm spread the He over a depth range of 300–1000 nm in such a way as to maintain a constant He/dpa ratio of 0.22 for Fe-Cr alloys and 1.0 for alloy 800H. Dual beam irradiation details are provided in Ref. [21]. Fig. 2 shows the Fe and He concentration and damage vs. depth profiles in alloy 800H for the case of 3.74×10^{16} i/cm^2 (17 dpa) at 600 nm depth and 1.0 He/dpa using SRIM [20] in quick Kinchin-Pease mode with a displacement energy of 40 eV.

Nuclear reaction analysis (NRA) was selected as the principal measurement technique because of the proximity of the ion beam

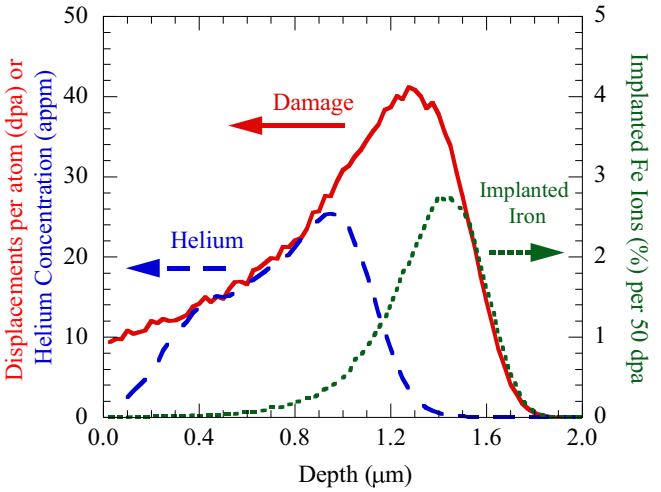

Fig. 2. Iron and helium depth profiles for the irradiated conditions in Fig. 1 using 5 MeV Fe^{2+} and degraded 2.15 MeV He^{2+} in alloy 800H to 3.74×10^{16} i/cm^2 (17 dpa) at 600 nm and with 1.0 He/dpa between 300 and 1000 nm depth.

Table 1
Compositions of alloys 800H and HT9 in at.%

	Composition (at.%)																
	Fe	Cr	Ni	C	P	S	N	O	Al	Cu	Mn	Mo	Nb	Si	Ti	V	W
800H heat 35175	45.7	21.5	29.0	0.34	0.01	0.001	0.03	0.01	1.14	0.64	0.74	0.037	0.002	0.31	0.39	0.042	0.002
HT9 heat 84425	83.9	12.5	0.48	0.99	0.01	0.005	0.04				0.50	0.59		0.41		0.36	0.15

analysis line in the Michigan Ion Beam Laboratory, providing rapid turnaround following an irradiation. The depth distribution of carbon in the samples was studied using the $^{12}C(d,p_0)^{13}C$ nuclear reaction. All measurements were performed using the 1.7-MV Tandetron accelerator of the Michigan Ion Beam Laboratory [22] at the University of Michigan. A deuterium ion beam of energy 1.5 MeV and normal to the sample surface was selected to maximize carbon detection in the depth range down to 3 μm from the sample surface [23]. A silicon surface barrier detector used to collect the spectrum at a scattering angle of 170° with a solid angle of 3.2 msr. No filter foil was used in front of the detectors, thus each detector collected Rutherford Backscattering (RBS) and NRA events. The samples were mounted on a sample holder attached to a five axis goniometer controlled by stepper motors. Most of the samples in this study were in the shape of 20 mm long bars of width 1.5 mm that were mounted on the sample holder with the length in the vertical direction. Due to the small sample width compared to the size of the focused beam on the sample (about 3 mm FWHM) the ion beam was carefully collimated using a 1 mm diameter aperture located 3 m in front of the sample and a double slit system located 30 cm in front of the sample. Both slits were adjusted so that the entire beam was on the sample and away from the edges. For example, in the case of 1.5 mm wide bars, the opening of the vertical slit was 0.6 mm ensuring a beam size in the vertical direction on the sample not bigger than 0.8 mm. The typical beam current on the samples was about 10 nA and the acquisition time was about 12 h.

The spectra were analysed using the code SimNRA 6.06 [24] and the $^{12}C(d,p)^{13}C$ reaction cross-section was calculated using SigmaCalc 2.0 [25]. The product of the number of ions and solid angle of the detector was obtained by fitting the high energy edge of the RBS events in the spectra. The carbon depth profile was determined to a maximum depth of about 3 μm with a depth resolution of 200 nm at the sample surface and 360 nm at a depth of 3 μm from the surface. The thickness of each layer was adjusted to the depth resolution according to the layer depth in the target. The final carbon depth profile results from adjusting the C concentration in each layer to match the number of counts between the SimNRA simulation and the spectrum.

Non-Rutherford elastic backscattering (EBS) [26] was used to measure the carbon content in a 100 nm Al_2O_3 coated Si sample. For this purpose a He^{2+} ion beam at 4335 keV was used to optimize the carbon sensitivity in the first 500 nm in the Si substrate using the resonant cross section that peaks at 4265 keV [27]. For this measurement, the same detector geometry was used as in the case of the NRA measurements with a beam incident angle of 0°. SimNRA 6.06 was used for spectrum analysis. The $^{12}C(\alpha,\alpha)^{12}C$ scattering cross-section was calculated with SigmaCalc 2.0.

Because the carbon profile in the sample shown in Fig. 1 suggests both incorporation of carbon and a redistribution of carbon, it was necessary to separate these two processes during the development of solutions to the uptake phenomenon. This was done by applying a thin (100 nm) coating of alumina by atomic layer deposition (ALD) at 150 °C. An argon over pressure was used to provide an inert environment before the deposition began. Trimethylaluminium (TMA, $Al_2(CH_3)_6$) was bubbled into the chamber and reacted with dangling hydroxyl (OH) groups on the surface of the substrate. The TMA was then pumped out of the chamber. After the TMA was removed, water was bubbled into the chamber and reacted with the dangling methyl (CH_3) groups to produce methane and alumina. Similar to the TMA, the water was pumped out of the chamber. This process was repeated for 980–1000 cycles resulting in a 100 nm thick layer on the surface. By virtue of the low solubility for carbon, the thin alumina layer acts as a barrier to carbon uptake from the environment. However, if carbon is in the beam, it will not affect its incorporation. Thus, by eliminating the uptake of carbon from the environment it can be verified that the beam is not the source of carbon. In this way, it also serves as a means to verify the effectiveness of proposed mitigation strategies.

3. Results and discussion

3.1. Carbon in the beam

While unlikely, consideration was given to the possibility that carbon is a component of the accelerated Fe^{2+} ion beam. The beam is an unlikely source of carbon since the beam is filtered using bending magnets both before the accelerator as low energy (20–30 keV) ions emerging from the source, and after the accelerator as high energy ions. Fig. 3a shows the abundance of the various masses of negative ions from the sputter source using both Fe and FeO targets. The Fe target yields a relatively low current of mass 56 amu compared to that for the 68 amu FeC ion and the 72 amu FeO ion. Injection of FeC into the accelerator brings in carbon, and injection of FeO also carries the possibility of bringing C_6 into the accelerator. The formation of carbon molecules up to large

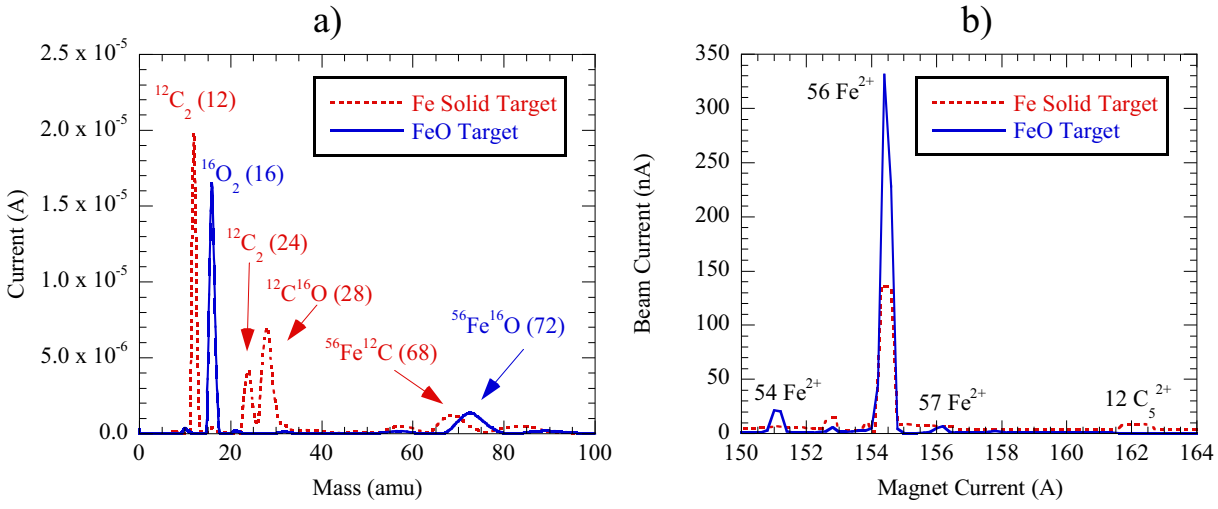

Fig. 3. a) Beam current vs. mass for species generated from Cs ion sputtering in a SNICS ion source using either solid Fe or FeO as the target material, and b) beam current of various ions vs. magnet current for the high energy magnet with a terminal voltage of 1.56 MV.

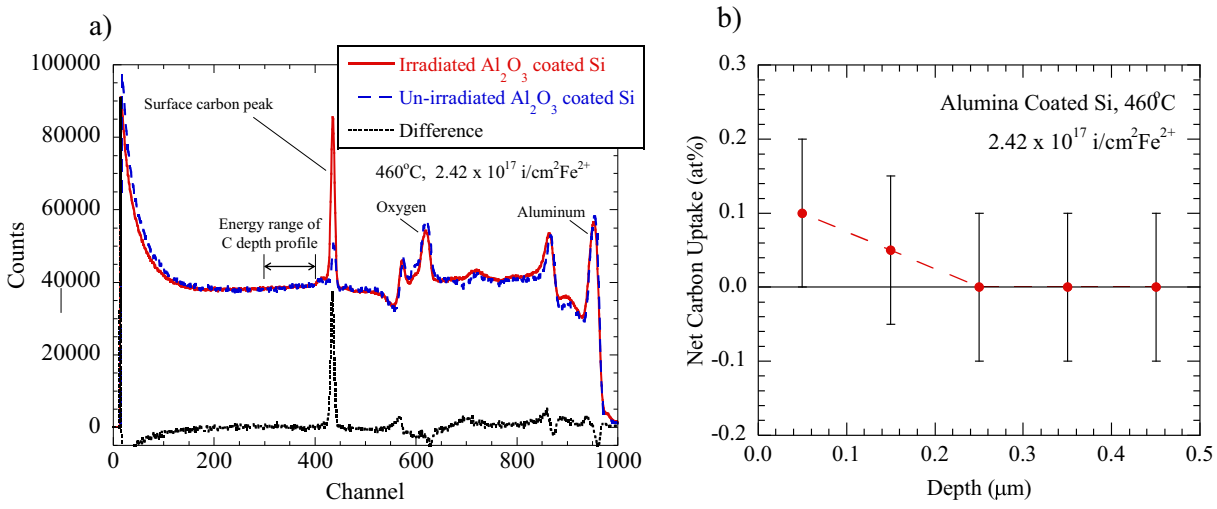

Fig. 4. EBS spectra of alumina coated Si a) in the non-irradiated and irradiated (5 MeV Fe^{2+} to 2.42 × 10^{17} i/cm^2 at 460 °C) conditions, and b) carbon depth profile determined from the difference in the spectra in a). Error bars represent the detection limit of the technique for C.

molecular weights is theoretically possible in a Cs sputter source [28].

However, Fig. 3b shows that the Fe^{2+} peak is far from the closest carbon molecule (C_5). At 1.56 MV, this separation is approximately 7.5 A of magnet current with a resolution of ~0.01 A. Therefore, it is not possible that carbon molecules are accelerated along with the beam.

To verify that no carbon is incorporated into the ion beam, a silicon wafer coated with alumina was irradiated with 5 MeV Fe^{2+} to a fluence of 2.42 × 10^{17} i/cm^2 and analyzed using EBS. Fig. 4a shows the EBS spectra of non-irradiated and irradiated samples, as well as the difference between the spectra. Aluminum and oxygen peaks from the alumina coating, the carbon peak from surface carbon, and the spectra energy range used to determine the carbon depth profile are marked. Fig. 4b shows carbon depth profile obtained from the spectrum difference in Fig. 4a. Within the experimental error (0.1 at.%) there is no evidence of carbon incorporation during the irradiation. A confirmation experiment was conducted on alumina coated, high purity Ni containing 0.002 at. % C irradiated to 1.21 × 10^{17} i/cm^2. As shown in Fig. 5, the net carbon uptake, plotted as the difference in the carbon depth profiles before and after irradiation, shows no evidence of incorporation of C from the beam.

3.2. Vacuum system and sample handling

Steps were then taken to ensure a clean beamline and target chamber. Beyond the high energy magnet, the beamline and target chamber are cryopumped. Either a turbopump backed by an oil-less roughing pump or a dry scroll pump were used initially to drop the pressure prior to cryopumping. Hence, all sources of oil anywhere in the vacuum system of the beamline or target chamber were removed. Further the chamber and sample stage were baked prior to irradiation and a pressure of <1 × 10^{-7} torr was achieved prior to sample heating and irradiation. The final sample preparation step consisted of cleaning with pure ethanol rather than denatured ethanol, which contains hydrocarbon chains. As shown by comparison of Figs. 6 and 1a, there was essentially no effect of

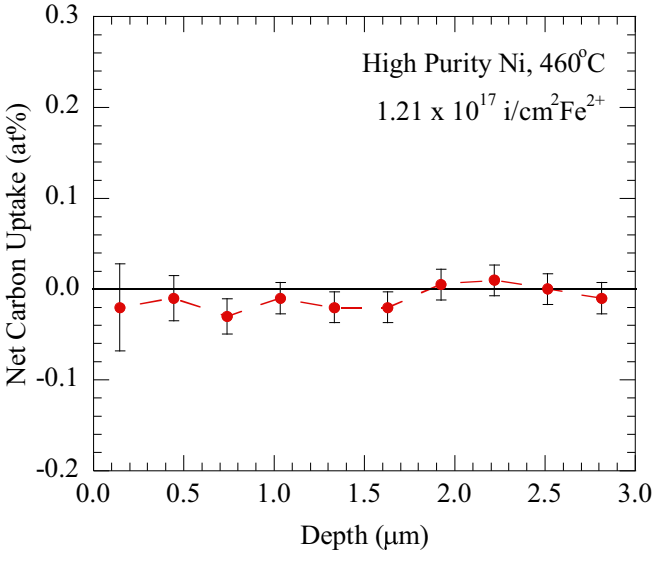

Fig. 5. Difference in carbon concentration profiles before and after irradiation of alumina coated, high purity Ni with 5 MeV Fe^{2+} to a fluence of 1.21 × 10^{17} i/cm^2 at 460 °C.

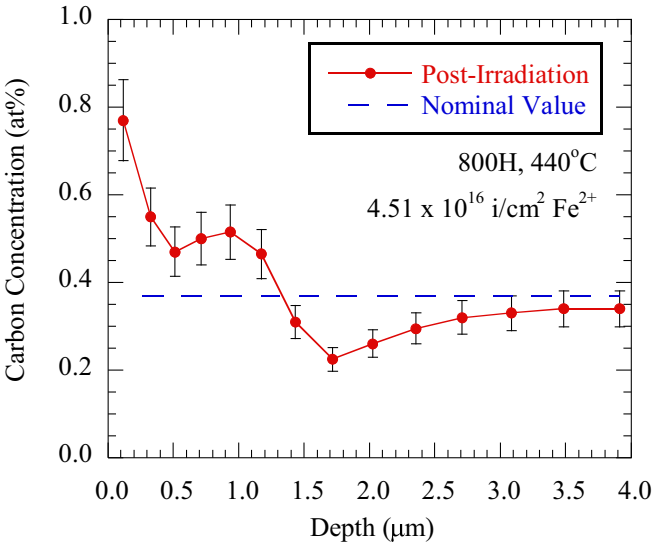

Fig. 6. Carbon concentration vs. depth profile in alloy 800H following irradiation with 5 MeV Fe^{2+} to 4.51 × 10^{16} i/cm^2 (20 dpa) at 440 °C.

these measures on the uptake of carbon during irradiation. Thus, the source of the carbon must be the residual gases in the vacuum system, and perhaps hydrocarbons adsorbed on the sample surface. Note that in Fig. 6 and subsequent plots of the composition vs. depth profiles, the surface peak was removed to focus on the carbon incorporation in the solid.

3.3. Cold trap and plasma cleaning

If residual gasses in the chamber and/or adsorbed onto the sample surface are the source of carbon, then plasma cleaning of the sample to remove hydrocarbons from the surface accompanied by a cold trap should eliminate the problem. The electron microscopy community has dealt with this problem for years and there are many references that document the source of carbon and the techniques to minimize its buildup on the surface and/or absorption into the samples [29–31]. Of the methods shown to reduce carbon buildup on both SEM and TEM samples, plasma cleaning and a cold trap are the most effective. Plasmas containing oxidizing species have been shown to be very effective at removing both hydrocarbons and any previously deposited carbon contamination [32–36]. Air, pure oxygen, oxygen/argon and oxygen/hydrogen mixtures have all been used with considerable success. In this case, samples were plasma cleaned in the chamber using an Evactron EP Series Plasma De-Contaminator. The device produces an active plasma in a remote chamber using radio frequency energy and transfers the active species to the cleaning chamber via gas flow. Room air acts as a source of oxygen to create reactive radicals and crack hydrocarbon chains. The oxygen radicals then combine with the broken hydrocarbons to form H_2O, CO, and CO_2, which are easily pumped by the vacuum system. Plasma cleaning performed in this study used a forward power of 15 W to clean the chamber and samples for 8 h prior to each experiment. Fig. 7a shows the effect of plasma cleaning on the carbon depth profile. Note that it is very effective in removing carbon incorporation into the sample by removing carbon from the sample and stage surfaces prior to irradiation.

The effect of using a liquid nitrogen cold trap is shown in Fig.7b. The cold trap consisted initially of a copper plate located about 5 mm from the sample surface at its closest point with a surface area of about 270 cm^2. It has since been designed to provide a cone-shaped surface with edges perpendicular to the sample and an area of 800 cm^2. The presence of the cold trap did not inhibit temperature control of the sample, and the high sample temperature did not warm up the cold trap as verified with thermocouples. Note here that the cold trap is also very effective, indicating that condensation of hydrocarbons on the cold surface near the sample can effectively prevent incorporation into the sample during irradiation. Finally, Fig. 7c shows the effectiveness of both techniques together.

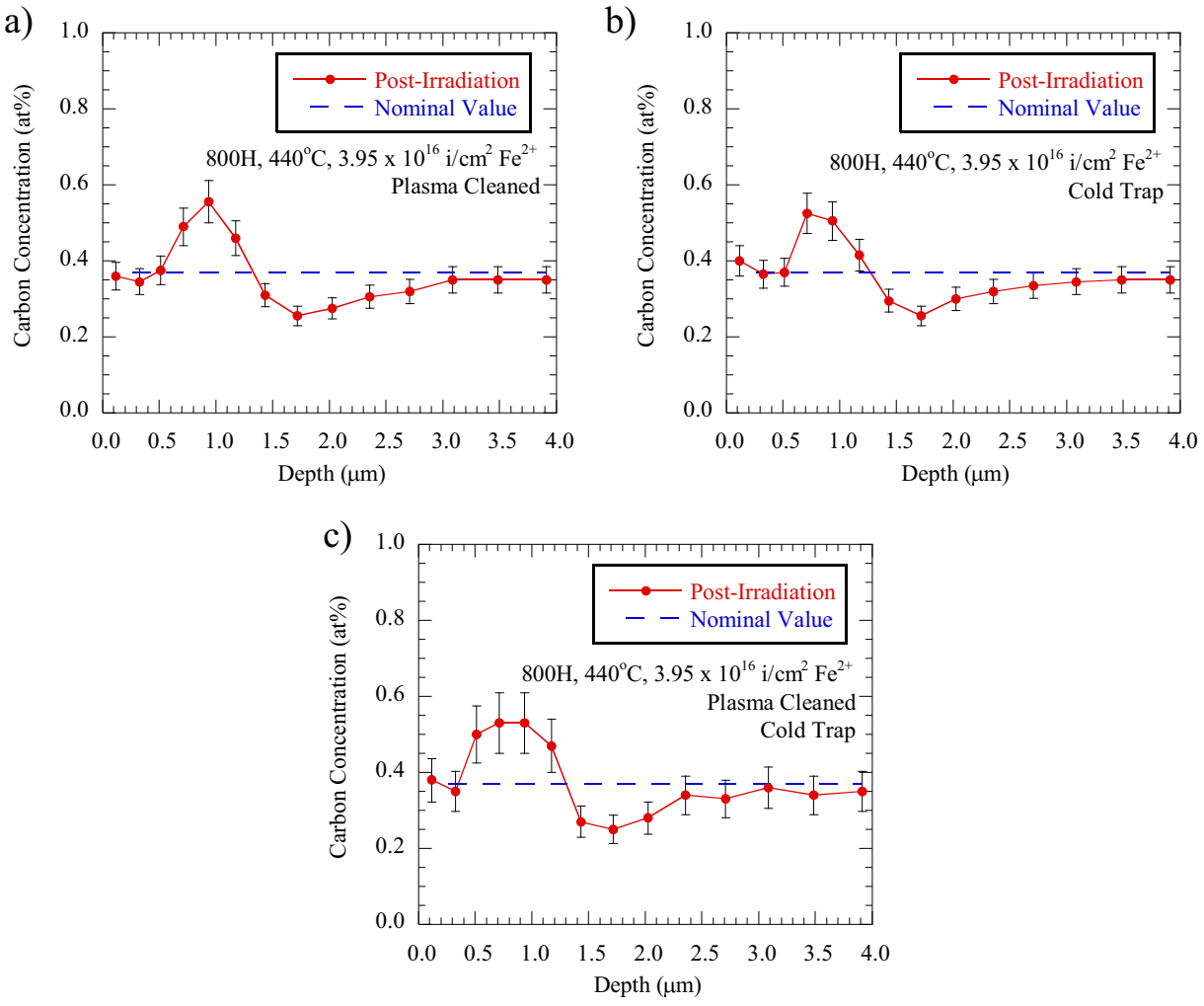

Fig. 7. Carbon concentration vs. depth profile in 800H following irradiation with 4.4 MeV Fe^{2+} to 3.95×10^{16} i/cm^2 (20 dpa) at 440 °C after a) plasma cleaning prior to irradiation, b) irradiation with a liquid nitrogen cold trap, and c) the combination of both plasma cleaning and a cold trap.

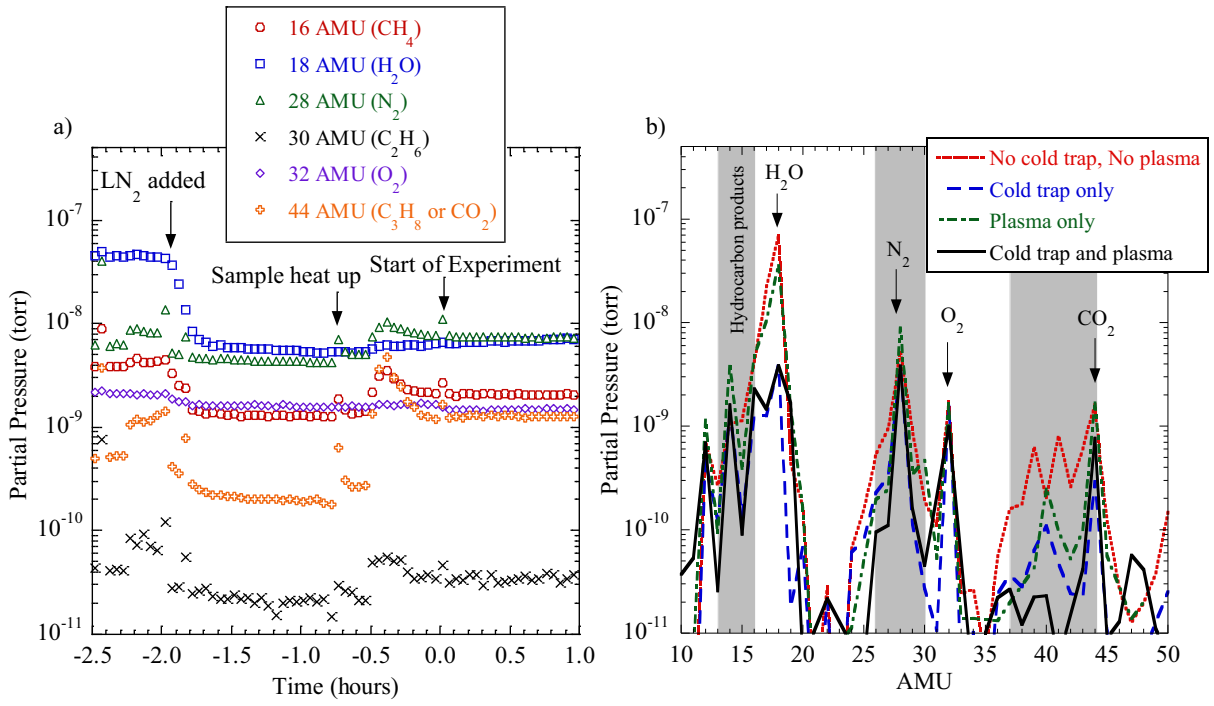

Fig. 8. Partial pressures of selected gasses in the vacuum a) as a function of time after plasma cleaning and cooling of the cold trap, and b) as a function of amu for different procedures.

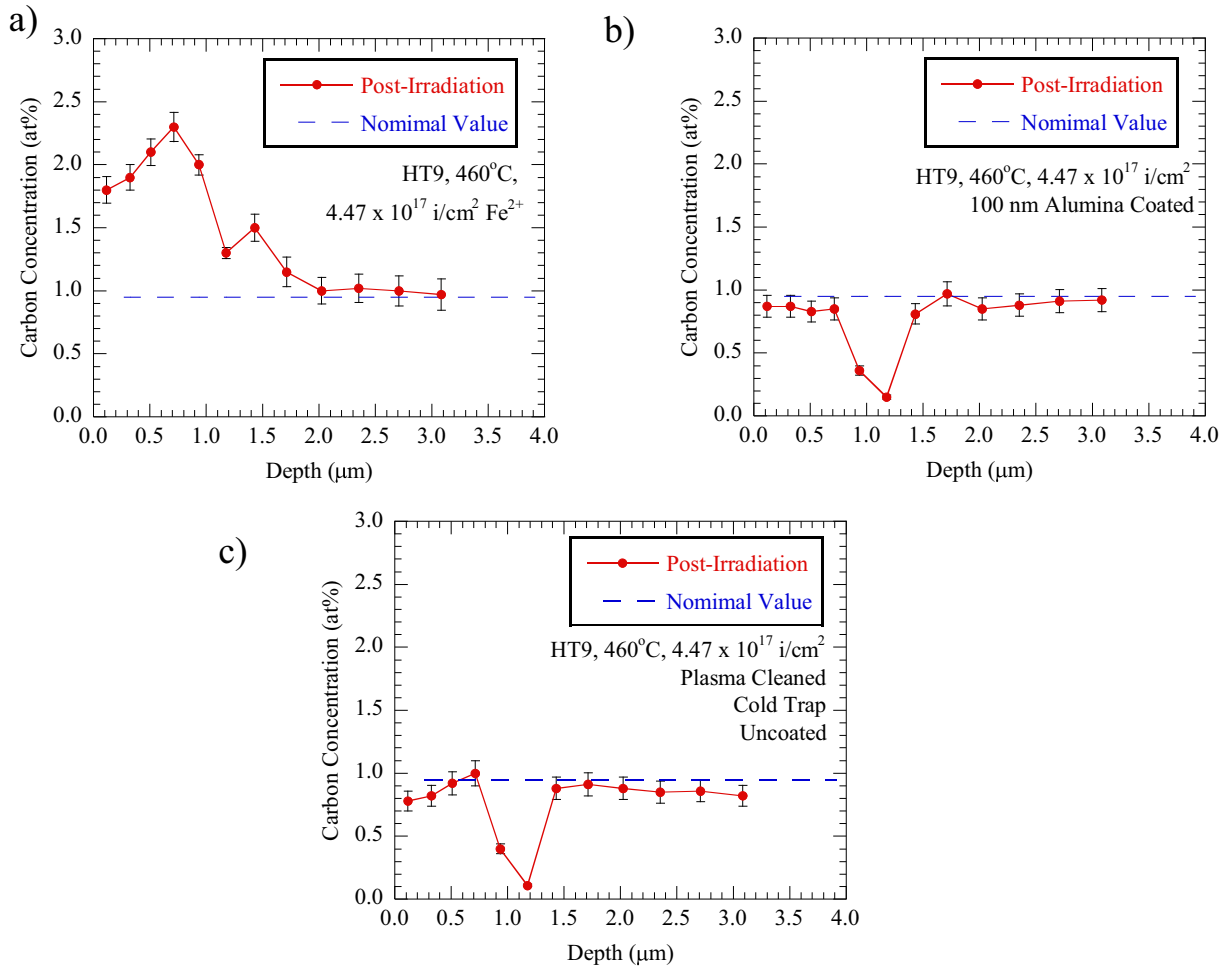

Fig. 9. Carbon concentration profile for alloy HT9 following dual ion irradiation with 5 MeV Fe^{2+} to 4.47 × 10^{17} i/cm^2 (188 dpa) and 2.15 MeV He^{2+} to 6 × 10^{12} i/cm^2 at 460 °C, a) prior to institution of carbon control measures, b) with a 100 nm alumina coating, and c) on a bare sample following plasma cleaning and use of the cold trap.

Fig. 8 shows the effectiveness of plasma cleaning in combination with a cold trap in reducing carbon-containing molecules in the vacuum. Fig. 8a shows the partial pressures of various species upon addition of LN_2 to the cold trap. The partial pressures measured by the RGA are referenced to the total pressure measured by an independent ion gage. Note that the partial pressure of water vapor drops by one order of magnitude upon addition of LN_2, as expected. Other species such as CH_4 (16 amu), N_2/CO (28 amu), C_2H_2 (30 amu), and C_3H_8/CO_2 (44 amu) drop significantly, but as expected, O_2 (32 amu) is largely unaffected. Fig. 8b shows the partial pressure in the target chamber as a function of specie. The grey bands indicate the hydrocarbon products that could result from break up of CH_4 (left most band), C_2H_2 (center band), and C_3H_8 (right most band). Note that in all three cases both the cold trap and plasma cleaning had significant effects, especially for molecules of high molecular weight. The signals at amu 39 and 41 can result from breakdown of larger hydrocarbon chains in the RGA unit. Both were reduced with the both plasma cleaning and the cold trap, indicating the effectiveness of these measures on large hydrocarbons. These results show that exotic schemes [37,38] are unnecessary if hydrocarbons are immobilized and/or removed from the vacuum system for the duration of the experiment.. Also note that the water vapor pressure was significantly reduced by the cold trap but not plasma cleaning, as expected. Further, neither affected the N_2 or O_2 partial pressures, also as expected.

While the efficacy of these mitigation techniques was established on alloy 800H, experiments were also conducted on alloy HT9, a Fe-12Cr-1Mo ferritic-martensitic alloy. These irradiations were conducted with 5 MeV Fe^{2+} ions to a dose of 4.47×10^{17} i/cm^2 (188 dpa) at 460 °C. Fig. 9a shows the carbon concentration depth profile for a bare sample without either plasma cleaning or use of a cold trap. Note that there is significant carbon uptake in the surface of the sample following this irradiation. Results of the same irradiation are shown for an alumina-coated (Fig. 9b) and bare (Fig. 9c) samples irradiated simultaneously in the chamber following plasma cleaning and with use of the LN_2 cold trap. Note that there is no change in the carbon level near the surface. But what is revealed is a significant change in the carbon content at the location of the damage peak and the iron ion range. The source of the drop in carbon is the subject of a subsequent paper.

4. Conclusions

Experiments on high purity Si and Ni, and alloys 800H and HT9 coated with alumina establish that incorporation in the ion beam is not the source of carbon contamination during heavy ion irradiation. Uptake of carbon in ion irradiated samples is the result of adsorption under the beam of hydrocarbons that are present both in the vacuum system and on the surfaces of samples and mounting stages. Standard cleaning techniques are inadequate to remove enough hydrocarbons to prevent cracking of carbon molecules under irradiation followed by adsorption and then absorption during irradiation. Coating with a thin, 100 nm film of alumina is a very effective mitigation technique but may not always be practical. Both plasma cleaning prior to irradiation and use of a liquid nitrogen cold trap during irradiation effectively remove or immobilize the hydrocarbons, allowing for high temperature irradiation without the uptake of carbon. This is the first report of complete elimination of carbon uptake for high fluence, high temperature ion irradiation of iron-base alloys.

Acknowledgements

The authors wish to acknowledge support for this research from the Department of Energy, Office of Nuclear Energy under the Nuclear Engineering University Program, the Michigan Ion Beam Laboratory at the University of Michigan for providing facilities, and to Elaina Anderson and Emmanuelle Marquis for APT data on carbon in alloy 800H.

References

[1] P.R. Okamoto, S.D. Harkness, J.J. Laidler, ANS Trans. 16 (1973) 70.
[2] P.R. Okamoto, H. Wiedersich, J. Nucl. Mater. 53 (1974) 336.
[3] G. Schmitz, J.C. Ewert, F. Harbsmeier, M. Uhrmacher, F. Haider, Phys. Rev. B 63 (2001) 224113.
[4] F.A. Garner, J. Nucl. Mater. 177 (1983) 177–197.
[5] H.J. Matzke, P.G. Lucuta, T. Wiss, Nucl. Instrum. Meth. B 166–167 (2000) 920–926.
[6] G.S. Was, J.T. Busby, T. Allen, E.A. Kenik, A. Jenssen, S.M. Bruemmer, J. Gan, A.D. Edwards, P. Scott, P.L. Andresen, J. Nucl. Mater. 300 (2002) 198–216.
[7] G.S. Was, Z. Jiao, E. Getto, K. Sun, A.M. Monterrosa, S.A. Maloy, O. Anderoglu, B. H. Sencer, M. Hackett, Scripta Mater. 88 (2014) 33–36.
[8] G.S. Was, J. Mater. Res. 30 (9) (2015) 1158–1182.
[9] I.L. Singer, J. Vat. Sci. Technol. Al (1983) 419.
[10] I.L. Singer, T.M. Barlak, Appl. Phys. Lett. 43 (1983) 457.
[11] G.J. Thomas, W. Bauer, J. Vac. Sci. Technol. 12 (1975) 490.
[12] C.A. Carosella, I.L. Singer, R.E. Bowers, E.R. Gossett, Ion Implantation Metallurgy, Metallurgical Society of AIME, Warrendale, Pennsylvania, 1980, p. 103.
[13] J.A. Knapp, D.M. Follstaedt, S.T. Picraux, Ion Implantation Metallurgy (Metallurgical Society of AIME, Warrendale, Pennsylvania, 1980), p. 152, Appl. Phys. Lett. 37 (1980) 330.
[14] I.L. Singer, C.A. Carosella, I.R. Reed, Nucl. Instrum. Methods Phys. Res. 182/183 (1981) 923.
[15] J.A. Knapp, D.M. Follstaedt, and S, T. Picraux Appl. Phys. Lett. 37 (1980) 330.
[16] C.L. Gossett, Nucl. Instrum. Methods Phys. Res. 191 (1981) 335.
[17] G.K. Hubler, Nucl. Instrum. Methods Phys. Res. 191 (1981) 101.
[18] F.K. Naehring, A. Schmidt, J. Schoneich. Phys. Stat. Sol. (a) 44 (1977) K141.
[19] M.J.F. Healy, Nucl. Instrum. Methods Phys. Res. Sect. B 129 (1997) 130–136.
[20] J.F. Ziegler, M.D. Ziegler, J.P. Biersack, Nucl. Instrum. Methods Phys. Res. Sect. B 268 (2010) 1818–1823.
[21] S. Taller, D. Woodley, E. Getto, A.M. Monterrosa, Z. Jiao, O. Toader, F. Naab, T. Kubley, S. Dwaraknath, G.S. Was, Nucl. Instrum. Methods Phys. Res. Sect. B 412 (2017) 1–10.
[22] O. Toader, F. Naab, E. Uberseder, T. Kubley, S. Taller, G. Was, Phys. Proc. (2016), in press.
[23] D. Abriola, A.F. Gurbich, M. Kokkoris, Nucl. Instrum. Methods Phys. Res. Sect. B 301 (2013) 41–46.
[24] M. Mayer, Improved physics in SIMNRA 7, Nucl. Instrum. Methods Phys. Res. Sect. B 332 (2014) 176–180.
[25] A.F. Gurbich, Nucl. Instrum. Methods Phys. Res. Sect. B 371 (2016) 27–32.
[26] R.P. Cox, J.A. Leavitt, L.C. McIntyre Jr., Handbook of Modern Ion Beam Materials Analysis, MRS, Pennsylvania, 2009.
[27] J.A. Leavitt, L.C. McIntyre Jr., P. Stoss, J.G. Oder, M.D. Ashbaugh, B. Dezfouly-Arjomandy, Z.M. Yang, Z. Lin, Nucl. Instrum. Methods Phys. Res. Sect. B 40–41 (1989) 776.
[28] Middleton, R. (1989). A Negative-Ion Cookbook, http://www.pelletron.com/cookbook.pdf.
[29] D.R.G. Mitchell, Micron 73 (2015) 36–46.
[30] S. Hettler, M. Dries, P. Hermann, M. Obermair, D. Gerthsen, M. Malac, Micron 96 (2017) 38–47.
[31] C. Soong, P. Woo, D. Hoyle, Microscopy Today (Nov. 2012) 7–9.
[32] A. Griffiths, J. Phys. Conf. Ser. 241 (2010) 012017–012020.
[33] T.C. Isabell, P.E. Fischione, C. O'Keefe, M.U. Guruz, V.P. Dravid, Microsc. Microanal. 5 (1999) 126–135.
[34] C.M. McGilvery, A.E. Goode, M.S.P. Shaffer, D.W. McComb, Micron 43 (2012) 450–455.
[35] N.J. Zaluzec, Springer-Verlag, Heidelberg, New York, Berlin, 2001.
[36] N.J. Zaluzec, B.J. Kestel, D. Henriks, Microsc. Microanal. 3 (1997) 10–14.
[37] L. Shao, J. Gigax, D. Chen, H. Kim, F.A. Garner, J. Wang, M.B. Toloczko, Nucl. Instrum. Methods Phys. Res. Sect. B (2017), http://dx.doi.org/10.1016/j.nimb.2017.05.026.
[38] J. Gigax, H. Kim, E. Aydogan, F.A. Garner, S. Maloy, L. Shao, Mat. Res. Lett. (2017), http://dx.doi.org/10.1080/21663831.2017.1323808.